Electrochemical Degradation of Amoxicillin in Acidic Aqueous Medium Using TiO$_2$-Based Electrodes Modified by Oxides of Transition Metals

Jaxiry Shamara Barroso Martínez

Centro de Investigación y Desarrollo Tecnológico en Electroquímica SC: Centro de Investigacion y Desarrollo Tecnologico en Electroquimica SC

Antonia Sandoval González

Centro de Investigación y Desarrollo Tecnológico en Electroquímica SC: Centro de Investigacion y Desarrollo Tecnologico en Electroquimica SC

Mónica Cerro López

Universidad de las Américas Puebla: Universidad de las Americas Puebla

Fabricio Espejel Ayala

Centro de Investigación y Desarrollo Tecnológico en Electroquímica SC: Centro de Investigacion y Desarrollo Tecnologico en Electroquimica SC

Jesús Cárdenas Mijangos

Centro de Investigación y Desarrollo Tecnológico en Electroquímica SC: Centro de Investigacion y Desarrollo Tecnologico en Electroquimica SC

José de Jesús Treviño Reséndez

Centro de Investigación y Desarrollo Tecnológico en Electroquímica SC: Centro de Investigacion y Desarrollo Tecnologico en Electroquimica SC

Yunny Meas Vöng

Centro de Investigación y Desarrollo Tecnológico en Electroquímica SC: Centro de Investigacion y Desarrollo Tecnologico en Electroquimica SC

Juan Manríquez Rocha

Centro de Investigación y Desarrollo Tecnológico en Electroquímica SC: Centro de Investigacion y Desarrollo Tecnologico en Electroquimica SC

Erika Bustos Bustos (✉ ebustos@cideteq.mx)

Centro de Investigación y Desarrollo Tecnológico en Electroquímica, S. C.   https://orcid.org/0000-0003-0955-7684

Research Article

Abstract

One of the most widely used antibiotics is amoxicillin (AMX), which is the most widely used in humans and animals, but it is discharged metabolically due to its indigestibility. Conventional biological and physicochemical methods for removing AMX from water are not enough to mineralize it, only it is concentrated and transferred to produce new residues that require further processing to remove the new residues.

In this research, naked and modified surfaces with TiO_2 nanotubes ($TiO_{2,nt}$) electrophoretically modified with PbO_2, IrO_2, RuO_2, and Ta_2O_5 were used to evaluate their efficiency in the electrochemical degradation of AMX in acid media (0.1 mol L^{-1} H_2SO_4). After their comparison, Pb-Ta 50:50|$TiO_{2,nt}$|Ti showed the highest removal efficiency of AMX (44.71 %) with the lowest specific energy consumption (8.69 ± 0.78 kWh Kg COD^{-1}), and the average instant current efficiency of 26.67 ± 9.19 %, in comparison with the others naked and modified surfaces of $TiO_{2,nt}$|Ti.

1. Introduction

Due to the increase in the world's population, it is predicted that in the coming years the demand for healthy water will increase by 55 % (Gopinath et al. 2020; Suhaimy et al. 2020). Although industries treat their wastewater with conventional processes, these are not efficient in degrading all pollutants, especially emerging organic compounds (EOCs) (De la Cruz et al. 2013). EOCs are those organic pollutants that have not been recognized by existing environmental legislation, but it has been shown that these pollutants are affecting aquatic ecosystems and their environment (Bueno et al. 2012; Giwa et al. 2021; Majumder et al. 2019; Phoon et al. 2020; Rasheed et al. 2019). In the case of antibiotics, studies by Klein et al. (2018) found that from 2000 to 2015 their consumption increased by 65 % and that some of these antibiotics are only partially metabolized allowing a fraction of them to be excreted from the body in an unchanged form after consumption (Rasheed et al. 2019; Ye et al. 2019). The mode of use, types, and concentrations of antibiotics are not the same for all countries, there are concentrations from ppm to ppt, even after the wastewater has been treated (Wen et al. 2014), other studies show that antibiotics are present in different ecosystems (Wang and Zhuan 2020), although in low concentration, but they remain biologically active, causing long-term resistance of bacteria, generating a negative impact on human and animal health (Hou et al. 2019; Phoon et al. 2020).

One of the most widely used antibiotics is amoxicillin (AMX, $C_{16}H_{19}N_3O_5S$) (PubChem 2021; Wang and Wang 2016). In traditional biological wastewater treatment, AMX exhibits stable chemical properties, biological toxicity, and a low rate of biodegradation (Song et al. 2016). Conventional methods for removing antibiotics from water include coagulation (Bratby 2016), ozone (O_3) and O_3 - H_2O_2 (Bavasso et al. 2020), biological systems as activated sludge, membrane and sequential bioreactor (Wang et al. 2020), inverse osmosis (Baheri et al. 2016), and adsorption by activated carbon (Perrich 2018), the disadvantage being that these contaminants are not mineralized, but only concentrated and transferred

to produce new residues that require further processing to remove the new residues. In some works, amoxicillin mineralization has been reported by different methods: using TiO_2 activated carbon composites, 50 to 100 % of 50 mg L^{-1} of amoxicillin at pH 3 to 10 was removed with sunlight for 180 min (PubCHem 2021). Using TiO_2 nanotubes with graphite and adding $KBrO_3$ a degradation of almost 100 % is achieved (Gar et al. 2016). With hybrid processes: ultrafiltration membrane, activated carbon adsorption, and ultrasound irradiation in 10 ppm of amoxicillin, 99.5 % were removed (Secondes et al. 2014); and with adsorption, membrane and ultrasound irradiation for 0.1 mg L^{-1}, 99 % was removed (Naddeo et al. 2020).

Advanced oxidation process (AOPs) with modified electrodes are other promise technology, which shows high removal percentages of pharmaceutical compounds as paracetamol (Brillas et al. 2005), metoprolol (Dirany et al. 2012), sulfachloropiridazine (Cavalcanti et al. 2013), omeprazole (García-Segura et al. 2014), chloramphenicol (Olvera-Vargas et al. 2014), ranitidine (Salazar 2014), phantetra (Panizza et al. 2014) and amoxicillin (León et al. 2020). The oxidant power of AOPs is determined by the high oxidation overpotential to O_2 evolution and the sorption enthalpy of electrogenerated hydroxyl radicals (Marcelino et al. 2017; Sopaj et al. 2015; Tan et al. 2020; Zha et al. 2014). AOPs are used because of their rapid reaction rate and strong oxidation capacity, which are effective for antibiotic degradation in aquatic environments (Benjedim et al. 2020; Moura et al. 2018; Seo and Park 2009; Wang and Zhuan 2020). In AOPs are used the dimensional stable anodes (DSA®), which are constructed by a thin film of transition metal oxides over metal as titanium (Ti) by its low cost; the Ti is sandblasted to increase the exposed area to include the metallic oxides, as it has been reported previously (Herrada et al. 2016, 2018, 2020; León et al. 2020).

In the case of nanostructured TiO_2, it is used because it has a relatively high quantum value, easy accessibility, low toxicity, high physical/chemical stability, large surface area, fast degradation rates, is non-toxic, is biocompatible with the environment, and can be easily synthesized (Gopinath et al. 2020; Molina-Reyes et al. 2020). TiO_2 nanotubes can be obtained by different synthesis methods, (a) hydrothermal (Subramanian et al. 2020), anodization (Diao et al. 2020; Suhaimy et al. 2020), microwave (Martínez-Sánchez et al. 2019), impregnation (Kulkami et al. 2016), sol-gel (Muswareen et al. 2019), solvothermal (Oh et al. 2019), template synthesis, and chemical reduction (Peng et al. 2021). Anodization is considered the most convenient and effective method for preparing high-quality TiO_2 nanotubes due to its good controllability, simple operation, low cost, and environmental friendliness (Liu et al. 2013). Currently, there are several researches focused on modifying TiO_2 nanotubes with different materials, for example TiO_2-Ru (Gopinath et al. 2020), Co/Bi/TiO_2 NTA (Ahmadi and Wu 2020), TiO_2-S (Yang et al. 2021), Co-TNT (Caia et al. 2020), TiO_2 NTA/Cu_2O (Koiki et al. 2020), Fe-TNT (Subramaniam et al.2020), TNT/Fe_3O_4/TiO_2 (Chen et al. 2018), TNTs@GO (Lei et al. 2018), TiO_2/SiO_2 (Raseed et al. 2019), g-C_3N_4/Ti_3C_2/TiO_2 (Diao et al. 2020), TiO_2/NTs/AgBr/BiOBr (Ye et al. 2018), Ag/TNA (Peng et al. 2021), CeO_2 (Koiki et al. 2020), doped Zn (Xu et al. 2005), N_2 (Lin et al. 2011), SnO_2 (Tsai et al. 2017), CdS (Zhang et al. 2018), CdSe (Zhang et al. 2009), PbS (Zhang et al. 2016), and Pt (Zhou et al. 2018). Most of

these nanomaterials have been used for the degradation of dyes or other organic compounds, these TiO_2 doped nanotubes have not been proposed to degrade amoxicillin.

In this research, naked and modified surfaces with TiO_2 nanotubes ($TiO_{2,nt}$) electrophoretically modified with PbO_2, IrO_2, RuO_2, and Ta_2O_5 were used to evaluate their efficiency in the electrochemical degradation of AMX in aqueous media, which is an example of the EOCs, and it has not been reported before. This pharmaceutical product has been electro-oxidized using IrO_2-Ta_2O_5|Ti and RuO_2-Ta_2O_5|Ti in acid (0.1 mol L^{-1} H_2SO_4) and neutral (0.1 mol L^{-1} Na_2SO_4) media in a previous study (Sopaj et al. 2015). On this occasion, the $TiO_{2,nt}$ modified with IrO_2-Ta_2O_5, RuO_2-Ta_2O_5, and PbO_2-Ta_2O_5 are considered to electrooxidize AMX in acid media (0.1 mol L^{-1} H_2SO_4).

2. Experimental Section

2.1. Preparation of modified electrodes.

Titanium alloy grade 2 (ASTM B265) was used in this study by its excellent balance of strength, ductility, toughness, and wieldable; this material shows corrosion resistance in highly oxidizing and mildly reducing environments (ITA 2005). Ti plates were modified to morphological characterization 3.0 cm in height, 1.0 cm in width, and 0.1 cm in thickness (Fig. 1A). Ti cylinders were also modified to AMX electro-oxidation, they were 0.7 cm in diameter and 5.0 cm in height (Fig. 1B).

The Ti plates and cylinders were anodized to form TiO_2 nanotubes ($TiO_{2,nt}$) by a voltage application of 30 V for 1, 2, 3, and 4 h (Cerro-López et al. 2014) and then modified with the different oxides deposits and their combinations. The growth of TiO_2 nanotubes is carried out by (a) the formation of the barrier layer, (b) the oxidation of titanium and (c) the dissolution of Ti, which is related to the concentration of F- ions. At the beginning of the anodization, 0.5 mA is recorded; after 2 min, this current drops to 0.3 mA, and after 5 min, 0.1 mA is obtained. The current drop is attributed to the oxidation of Ti to form TiO_2. The current increases slightly with time but has fluctuations due to the competition between the growth of the titanium dioxide tubes and the dissolution of the oxide for the formation of stable tubes (Sreekantan et al. 2009; Sun et al. 2009; Zhao et al. 2005).

These deposits were: IrO_2 − Ta_2O_5 (Ir-Ta), RuO_2 − Ta_2O_5 (Ru-Ta) and PbO_2 − Ta_2O_5 (Pb-Ta) with the combinations 100:0, 70:30, 50:50, 30:70 and 0:100. In these experiments, a DC-power supply model GP-4303DU was used with a constant stirring rate of 300 rpm considering the $TiO_{2,nt}$ over Ti as working electrode, and a Ti plate or mesh as counter-electrode for the Ti plate and cylinder, respectively, considering 1 cm of separation between working and counter-electrode (Fig. 1).

To get the $TiO_{2,nt}$, a mechanical pre-treatment of the Ti surfaces was made with the polishing paper of 120, 240, 360, 1500, and 2000 particles inches-2 in presence of water, and finally with alumina (Al_2O_3) of 0.3 mm of diameter with a polishing cloth. All these modified surfaces were cleaned by ultrasound in

acetone, ethanol, and deionized water for 10 min in each solvent. In all cases, the modified electrodes were rinsed with deionized water and dried with nitrogen.

To modify the $TiO_{2,nt}$ by electrophoretic anodization with PbO_2 and Ta_2O_5 in a relation v/v of 100:0, 30:70, 50:50 and 70:30, the precursors solutions used were 0.5 mol L^{-1} $Pb(NO_3)_2$ (Meyer, 99 %) in 0.1 mol L^{-1} HNO_3 (J. T. Baker, 70 %) and 1.0 mol L^{-1} $TaCl_5$ (Strem Chemicals, 99.9 %) in isopropanol (Karal, 99.5 %) (Herrada et al. 2016, 2018, 2020; Trasatti and Petrii 1991) applying a current density of 50 mA cm^{-2} by 5 s (León et al. 2020) in a two electrodes electrochemical cell, where the Ti plate or cylinder was the working electrode with a Ti plate or mesh as counter-electrode, respectively (Fig. 1).

To modify the $TiO_{2,nt}$ by electrophoretic anodization of Ir, Ru, and Ta a current density of 20 mA cm^{-2} by 20 min with constant stirring (300 rpm) was used, the precursors' solutions used were 0.1 mol L^{-1} H_2IrCl_6 (Stream Chemicals, 99.9 %) in 50 % HCl (J. T. Baker, 38 %) and isopropanol (Karal, 99.5 %) in a relation 2:1; in the case of Ru deposition, 0.1 mol L^{-1} $RuCl_3 \cdot H_2O$ (Strem Chemicals, 99.9 %) in 50 % HCl and isopropanol 2:1, and 1 mol L^{-1} $TaCl_5$ (Strem Chemicals, 99.9 %) in isopropanol under vigorous stirring.

The Ru-Ta and Ir-Ta ratios employed in the precursors' solutions were 100:0, 30:70, 50:50, 70:30 and 100:0 v/v in a two electrodes electrochemical cell, where the Ti plate or cylinder was the working electrode with a Ti plate or mesh as counter-electrode, respectively (Fig. 1), which were used in the electrodeposition as it has been reported before (Herrada et al. 2018, 2020; León et al. 2020). After electrophoretic deposition of Ru-Ta and Ir-Ta with the different ratios, the synthesis of metal oxides was obtained in two-step thermal decomposition, 523 K for 10 min, and 723 K for 1 h (Herrada et al. 2018, 2020; León et al. 2020).

During this study, before use the different modified electrodes in the different activities of morphological characterization and AMX electro-oxidation, they were polarized with a constant current of 10 mA by 5 min in 0.5 mol L^{-1} H_2SO_4 (J. T. Baker, 95.9 %) with a constant stirring (500 rpm).

2.2. Characterization of naked and modified electrodes.

The electrochemical characterization was performed to define the superficial surface area of the different naked and modified electrodes using a three electrodes cell with 0.1 mol L^{-1} H_2SO_4 (J. T. Baker, 98 %) as support electrolyte at 298 K, with Pt wire (BASi), Ag|AgCl 3M NaCl (BASi), and naked and modified Ti, as counter, reference, and the working electrode, respectively, using a BASi – Epsilon$^{®}$ potentiostat from Bioanalytical Systems Inc. In all these measures, the electrochemical cell was saturated with ultra-pure nitrogen (Praxair, grade 5.0) for 10 min to eliminate the oxygen. With this experimental set, the electroactive area (A_e) of the naked and modified cylindrical electrodes were calculated with the capacitance method, using the capacitive current of the double layer (C_{dl}) generated in presence of 0.1 mol L^{-1} H_2SO_4 between ± 10 mV around the equilibrium potential, in one cycle at 20, 40, 60, 80 and 100 mV s^{-1} (Gúlfen et al. 2020; Herrada et al. 2018 and 2020; León et al. 2020; Ren et al. 2015), and

roughness factor (R) was calculated by each electrode in the study by the division of geometric area (A_g) between electroactive area (A_e), as R = A_g /A_e (Herrada et al. 2018, 2020; León et al. 2020; Ren et al. 2015). All these results were evaluated by quadruplicate to $TiO_{2,nt}$.

The morphology of naked and modified electrodes was characterized by scanning electron microscopy coupled to energy-dispersive X-ray spectroscopy (SEM-EDX) using a Jeol JSM-6500LV equipment with 15 eV and EDS Bruker XFlash6I10 as the detector. EDS analysis was achieved in the center of each electrode taking in images at 2500 x, considering an area of a circle of 1.3 micrometers of radius and a depth of 1.2 micrometers.

2.3. Electrochemical degradation of amoxicillin using modified electrodes.

The AMX electrochemical oxidations were performed using a Ti cylinder naked and modified with Pb, Ir, Ru and Ta to have Pb-Ta 30:70, Pb-Ta 70:30, Ru-Ta 30:70, Ru-Ta 70:30, Ir-Ta 30:70, and Ir-Ta 70:30 as an anode, with a Ti mesh cathode around it (León et al. 2020). With the same configuration of the electrochemical cell and the different naked and modified electrodes, the corresponding hydrodynamic curves were made using 0.1 mol L^{-1} H_2SO_4 in the presence of 10 mg L^{-1} AMX (Across Organics) at 300 rpm using a two-electrode cell arrangement in presence of Ti mesh and the naked and modified Ti cylinders as counter and the working electrode, respectively.

For the construction of the hydrodynamic curves, from the cyclic voltammetry, were selected ten potentials from equilibrium potential to obtain different cronoamperometries with a constant potential of 0.01, 0.34, 0.67, 1.00, 1.34, 1.67, 2.00, 2.34, 2.67, and 3.00 V vs. Ag|AgCl 3M NaCl to get the final current density after five minutes of each electrolysis and construct the hydrodynamic curves with current density vs. constant potential by duplicate.

After the construction of the different hydrodynamic curves, the working current density for the AMX electrochemical degradation in 0.1 mol L^{-1} H_2SO_4 was selected. To the electrolysis of AMX, a potentiostat − galvanostat Epsilon BASi was used applying 100 µA cm^{-2} with 300 rpm, and the AMX electrochemical degradation was measured by UV-Vis spectrophotometry (Fig. 2A) with a PerkinElmer Lambda XLS equipment obtaining the calibration curve with the different spectra of samples (Fig. 2B), where the UV absorption characteristic of AMX is at 235 nm by the electronic transition π Ž π* of the aromatic ring of AMX (Gúlfen et al. 2020) in 0.1 mol L^{-1} H_2SO_4 and the representative equation is A (a.u.) = 6 x 10^{-5} (AMX mg L^{-1}) − 1 x 10^{-4} and R^2 = 0.9956. With this calibration curve, the removal efficiency of AMX (η %) was obtained with the initial concentration (C_0) and final concentration (C_f), as Eq. 1 shows.

$$\eta \% = \left(\frac{C_o - C_f}{C_o}\right) * 100 \qquad \text{Eq. 1}$$

AMX degradation was monitored by chemical oxygen demand (COD) analysis according to Method 8000 using the Reactor Digestion Method defined in the Hach Water Analysis Manual®. A colorimetric determination was carried out with units of mg L^{-1} of COD, defined as the number of mg of O_2 consumed per liter of the sample under the procedure conditions, which was programmed on the DR/2010 spectrophotometer. The procedure consisted of heating the sample for two hours with a potent oxidizing agent (potassium dichromate). The oxidizable organic compounds react, reducing the dichromate ion ($Cr_2O_7^{2-}$) to a green chromic ion (Cr^{3+}). Using a concentration from 0 to 150 mg L^{-1} $Cr_2O_7^{2-}$, the amount of remaining Cr^{6+} was determined and using a concentration from 0 to 150 mg L^{-1}, the amount of Cr^{3+} produced was determined.

COD analyses were done in triplicate, with samples extracted during electrolysis to determine AMX degradation after 120 min of electro-oxidation to evaluate the removal efficiency of COD using naked Ti and modified $TiO_{2,nt}|Ti$ by Ir, Ru, and Pb without and with Ta in a relation of 100:0, 70:30, 50:50, 70:30 and 100:0. AMX mineralization was monitored from the removal of total organic carbon (TOC), determined on a TOC analyzer Shimadzu apparatus (model TOC-L). The specific energy consumption (EC, kWh m^{-3}) during electrochemical treatment was calculated according to the Eq. 2 (Huang et al. 2017; León et al. 2020; Zavala Salazar 2011):

EC = (E_{cell} It) / (1000 V) Eq. 2

Where: E_{cell} = average potential difference between the anode and cathode during electrolysis [=] V; I = current [=] A; t = electrolysis time [=] h.

The specific energy consumption per unit of mass of COD (E_{sp} = kWh Kg COD^{-1}) was calculated from Eq. 3:

E_{sp} = (1000 E I t) / ($COD_{t = 0\ min}$ – $COD_{t = 400\ min}$) V_s Eq. 3

where: E = potential [=] V; I = electric current [=] A; t = electrolysis time [=] h; $COD_{t = 0\ min}$ = COD at the start of the electrochemical degradation process [=] mg L^{-1}; $COD_{t = 400\ min}$ = COD at the end of the electrochemical degradation process (mg L^{-1}); V_s = volumetric volume of the sample [=] L.

The instant current efficiency (ICE, %) was calculated from Eq. 4 considering the effectiveness and feasibility of AMX degradation (Huang et al. 2017; León et al. 2020; Zavala Salazar 2011):

$$ICE(\%) = \frac{F\,V_s\,(\Delta COD)}{8000\,I\,\Delta t}$$

Eq. 4

Where: F = Faraday constant [=] 96,485 C mol^{-1}; V_s = volume of the solution [=] L; ΔCOD = experimental COD decrease (mg L^{-1}) in the time interval t (h); I = current [=] A.

3. Discussion Of Results

3.1. Morphological characterization of naked and modified electrodes.

The naked Ti shows a presence of Ti (69.21 %), O (17.03 %), C (11.24 %), and Si (2.52 %), while the $TiO_{2,nt}$ shows the different composition of these elements (Table 1) with Ti (close to 30 %), O (close to 70 %), C (between 2 and 6 %) without the presence of Si because the anodization to construct the nanotubes eliminate the silica over the surface of titanium, with the decrease of carbon when increase the anodization time by the possible impurity in the same surface at 1 h (1.97 %), 2 h (6.34 %), 3 h (5.05 %) and 4 h (4.92 %).

Additionally, the relation of titanium and oxygen in the EDS of $TiO_{2,nt}$ is 1:2, this result validates the atomic composition of a compacted and disorganized film of TiO_2 showing nanotubular structures with a diameter of 50.10 ± 7.11 nm after 1h (Fig. 3A), 45.34 ± 7.01 nm after 2h (Fig. 3B), 47.42 ± 7.31 nm after 3h (Fig. 3C), and 48.77 ± 7.78 nm after 4h (Fig. 3D). When increasing the anodization time just to $TiO_{2,nt}$ 4 h (Fig. 3D), it shows regions without nanotubes, with major dispersion and disorder.

Figure 4 shows the Raman spectra of naked Ti and $TiO_{2,nt}$ at different anodization times, where there are five signals at shifts of 142, 204, 394, 514, and 632 cm^{-1}, corresponding to the vibrational modes E_{1g}, E_{2g}, B_{1g}, (A_{1g}, B_{1g}), and E_{3g} for anatase crystalline phase, respectively (González et al. 2019). Furthermore, the signals at shifts of 448 and 621 cm^{-1} were assigned to the vibrational modes E_g and A_{1g} for the rutile crystalline phase (Boda and Shah 2017). A comparative revision of SEM (Fig. 3), EDX (Table 1), and Raman spectroscopy (Fig. 4) result revealed that the electrochemical anodizing of Ti foils produced nanotubular structures of TiO_2 having a chemical composition with the predominance of anatase crystalline phase.

The peaks with a Raman shift of 448 cm^{-1} and 621 cm^{-1} are characteristic of the rutile phase of TiO_2, which are related to E_g, B_g, and A_g by symmetric stretching, symmetric bending, and asymmetric bending, respectively, by the O-Ti-O bonding (Boda and Shah 2017). From the SEM (Fig. 3), EDX (Table 1), and Raman (Fig. 4) analyses, it is evident that electrochemical anodization leads to the formation of nanotubular structures with a chemical composition in a major proportion of anatase phase and minor

presence of rutile phase. Additionally, the increase of anodization time is proportional to the increase of the anatase and rutile signals.

This result indicates that the anodization time is indifferent between 1 to 3 h as Raman shows (Fig. 4) with the same anatase and rutile proportion because at the fourth hour begins the disorganization of the nanotubular structures of $TiO_{2,nt}$. By these results, the selected anodization time was 1 h to continue the modification of $TiO_{2,nt}$ with the different concentrations of electro-catalyzers included in this study: Pb, Ir, Ru, and Ta.

3.2. Electrochemical characterization of naked and modified electrodes.

In the characterization of the different modified electrodes by the capacitance method (Trasatti and Petrii 1991) to define the electroactive area (Table 2), the Ru-Ta 50:50 shows the highest electroactive area (13.45 cm^2) and roughness (1.93) $\cong$ Pb (12.97 cm^2; 1.86) > Ru-Ta 70:30 (11.98 cm^2; 1.72) $\cong$ Ru-Ta 30:70 (11.54 cm^2; 1.65) > Ta (11.15 cm^2; 1.60) $\cong$ Ir-Ta 70:30 (10.88 cm^2; 1.56) > Ru (7.81 cm^2; 1.12) $\cong$ Pb-Ta 30:70 (6.58 cm^2; 0.94) > Ir-Ta 50:50 (6.25 cm^2; 0.90) > Ti (5.00 cm^2; 0.72), the other electrodes show less electroactive area than Ti: Ir-Ta 30:70 (4.03 cm^2; 0.58) $\cong$ Pb-Ta 70:30 (3.77 cm^2; 0.54) $\cong$ Pb-Ta 50:50 (3.71 cm^2; 0.53) > TiO_2,nt (3.12 cm^2; 0.45) $\cong$ Ir (2.56 cm^2; 0.37). These results show that $TiO_{2,nt}$ with the different concentration of electrocatalizers increase the A_e and R.

Cyclic voltammetry was obtained for each naked Ti and modified $TiO_{2,nt}$ with the different concentrations of Pb, Ir, Ru, and Ta in 0.1 mol L^{-1} H$_2$SO$_4$ at 20 mV s^{-1} (Figure 5), where the $TiO_{2,nt}$ with Pb and Ir showed the biggest potential windows (close to 3.2 V vs. Ag½AgCl 3M NaCl) than with Ru (close to 2.2 V vs. Ag|AgCl 3M NaCl). In the case of the cyclic voltammetry at 200 mV s^{-1} (Figure 6) all the electrodes show a potential window close to 3.2 V vs. Ag½AgCl 3M NaCl, where appeared different oxidation peaks at 0.5 V and 1.4 V vs. Ag|AgCl 3M NaCl, they are related with the change of the oxidation state of the electro catalyzers, while the potential window of naked Ti and $TiO_{2,nt}$ reaches up to 1.5 V vs. Ag|AgCl 3M NaCl, where the naked Ti showed minor O$_2$ evolution than $TiO_{2,nt}$. The electro catalyzers Ru and Ir have a similar electrochemical behavior by their physicochemical characteristics as metallic conductivity and crystalline structure of rutile, though Ru has the hexagonal close-packed (h.c.p.) structure, while Ir is a face-centered cubic (f.c.c) structure (Micheli et al. 1978).

In the particular case of $TiO_{2,nt}$ modified with Ir-Ta, the electrochemical process associated is related with the Eq. 5 and 6 (Micheli et al. 1978) with a proportional decrease of the current density with the decrease of the Ta concentration: Ir-Ta 30:70 > Ir-Ta 50:50 > Ir-Ta 70:30. In the first redox couple Ir^{+2}/Ir^{+4} (Eq. 5) with 0.20, 0.15 and 0.10 mA cm^{-2} for 0.7 V vs. Ag|AgCl 3M NaCl, and for the second couple Ir^{+4}/Ir^{+5} (Eq. 6) with 0.25, 0.20 and 0.12 mA cm^{-2} for 1.45 V vs. Ag|AgCl 3M NaCl. These results indicate that Ta is necessary to be present in this kind of electrode to increase the electronic transference as they are modified in this

study, despite Ta does not participate in the redox process (Comninellis and Vercesi 1991), it is only a protonic conductor (León et al. 2020).

$$Ir^{+2} \rightarrow Ir^{+4} + 2e^-$$ Eq. 5

$$Ir^{+4} \rightarrow Ir^{+5} + e^-$$ Eq. 6

In the case of the $TiO_{2,nt}$ modified with Ru-Ta, there are two electrochemical process associated by the electrocatalizer (Audichon et al. 2014). The first redox couple Ru^{+3}/Ru^{+4} (Eq. 7) in 0.6 V vs. Ag|AgCl 3M NaCl, with the major current density Ru-Ta 70:30 (0.1 mA cm^{-2}) than Ru-Ta 50:50 and Ru-Ta 30:70 (0.05 mA cm^{-2}). The second redox couple Ru^{+4}/Ru^{+6} (Eq. 8) in 1.3 V vs. Ag|AgCl 3M NaCl, where the electrode with Ru-Ta 70:30 showed the highest current density (0.15 mA cm^{-2}) than Ru-Ta 30:70 (0.1 mA cm^{-2}) and Ru-Ta 50:50 (0.08 mA cm^{-2}).

$$Ru^{+3} \rightarrow Ru^{+4} + e^-$$ Eq. 7

$$Ru^{+4} \rightarrow Ru^{+6} + 2e^-$$ Eq. 8
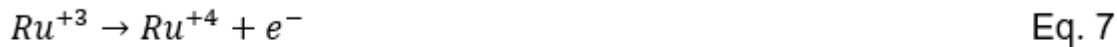
For $TiO_{2,nt}$ modified with Pb-Ta, there are two characteristics electrochemical process reported in the literature (Mahalingam et al. 2007), the first one is between 0.5 and 0.6 V vs. Ag|AgCl 3M NaCl by the redox coupled Pb^{+2}/Pb^{+3} (Eq. 9) with the same current density in the different concentrations of Pb-Ta (0.2 mA cm^{-2}); the second one between 1.5 and 1.6 V vs. Ag|AgCl 3M NaCl by the Pb^{+3}/Pb^{+4} (Eq. 10). In the last case, Ta is important for the electrocatalyst effect of Pb since Ta is a protonic conductor and is favorable to generate interfacial hydroxyl radicals for the electrocatalysis effect (León et al. 2020). In this case, Pb-Ta 50:50 showed the major current density (0.5 mA cm^{-2}) followed by Pb-Ta 70:30 (0.48 mA cm^{-2}); Pb-Ta 30:70 showed the lowest current density (0.35 mA cm^{-2}).

$$Pb^{+2} \rightarrow Pb^{+3} + e^-$$ Eq. 9

$$Pb^{+3} \rightarrow Pb^{+4} + e^-$$ Eq. 10

3.3. Electrochemical degradation of amoxicillin using modified electrodes.

Figure 7 shows the polarization curves of AMX in 0.1 mol L^{-1} H_2SO_4, where there are two characteristic zones related to kinetic control (from 0 to 1 V vs. Ag|AgCl 3M NaCl) and mix control (from 1 to 3 V vs. Ag|AgCl 3M NaCl). The mass transport zone was not defined by the possible effect of the nanotubular

structure of $TiO_{2,nt}$, which has different active sites without stabilizing a limit current density. After 2 V vs. Ag½AgCl 3M NaCl, there is an important increment in the current density by the electrolysis of water, at the same time, there are oxidant agents which are involved in the electroxidation of AMX in acid media, such as hydroxyl radicals (Auguste et al. 2016; León et al. 2020). The major current density achieved at 3 V vs. Ag|AgCl 3M NaCl was shown by Ir-Ta 100:0 (0.5 mA cm^{-2}) followed by: Ir-Ta 30:70 (0.18 mA cm^{-2}) > Ru-Ta 100:0 (0.16 mA cm^{-2}) > Ir-Ta 50:50 (0.14 mA cm^{-2}) > Ru-Ta 70:30 (0.12 mA cm^{-2}) > Ru-Ta 30:70 (0.08 mA cm^{-2}) > $TiO_{2,nt}$ @ Pb-Ta 70:30 @ Pb-Ta 50:50 @ Ir-Ta 70:30 @ Ta @ (0.07 mA cm^{-2}) > Ru-Ta 50:50 @ Pb-Ta 30:70 @ Ti (0.5 mA cm^{-2}) > Pb-Ta 100:0 (0.1 mA cm^{-2}).

With these results, 100 mA cm^{-2} was selected to be sure that electro-oxidation of AMX took place where the generation of hydroxyl radicals is developed (Herrada et al. 2018, 2020; León et al. 2020), with the highest oxidation redox state of the Ir (Eq. 6), Ru (Eq. 8) and Pb (Eq. 10). Figure 8 shows the removal efficiency of AMX (h%) in 0.1 mol L^{-1} H_2SO_4 every 10 min to 120 min of electrolysis. In this comparison, after 10 min the highest removal efficiency of AMX was shown with $TiO_{2,nt}$|Ti (25.57 %) modified by Pb-Ta 50:50 (44.71 %) which shows the highest current density in the polarization curve (Figure 7C) followed by Pb-Ta 30:70 (38.67 %) > Ir-Ta 50:50 (34.81 %) > Ru-Ta 50:50 (30.59 %) > Ir-Ta 100:0 (30 %) > Pb-Ta 70:30 (28.68 %) > Ta (22.91 %) > Ru-Ta 70:30 (22.50 %) > Ir-Ta 70:30 (20.81 %) > Ru-Ta 30:70 (17.59 %) > Ru-Ta 100:0 (14.60 %) > Ir-Ta 30:70 (10.94 %) > Pb-Ta 100:0 (0 %). In the case of the naked Ti, it shows a removal efficiency of 19.23 %.

Therefore, in this kind of surface, the inclusion of Ta plays an important role as it acts as a protonic conductor (Cominellis and Vercesi 1991; León et al. 2020) to promote the electro-oxidation of AMX by the major generation of ˙OH radicals when the protons are retained over the modified surface since, without Ta, the Pb-Ta 100:0 did not show any removal efficiency. Despite the Pb-Ta 50:50|$TiO_{2,nt}$|Ti and Pb-Ta 30:70 |$TiO_{2,nt}$|Ti electrode systems showed AMX removal, their removal efficiencies remain below from that achieved by the IrO_2-Ta_2O_5½Ti and RuO_2-Ta_2O_5½Ti electrode systems in acidic aqueous medium (i.e. 0.1 mol L^{-1} H_2SO_4) (León et al. 2020). A new revision of the CV responses compiled in Figure 6 revealed that the H_2O electro activation on the anatase $TiO_{2,nt}$ phase should occur at a potential more cathodic than for the other metallic oxide (MO). This difference in the ˙OH radicals generation (Eq. 11 and Eq. 12) seems to conduct to the ˙OH radicals deactivation via Eq. 13, which resembles the ˙OH radicals deactivation typically observed at photocatalytic anatase TiO_2 systems generating H_2O_2 (Eq. 14) (Zhang and Nosaka 2014).

$$H_2O + MO|TiO_2(H_2O)_{ads} \text{ Ž } _{ads}(H_2O)MO|TiO_2(˙OH)_{ads} + H^+ + e^- \quad \text{Eq. 11}$$

$$_{ads}(H_2O)MO|TiO_2(˙OH)_{ads} \text{ Ž } _{ads}(˙OH)MO|TiO_2(˙OH)_{ads} \quad \text{Eq. 12}$$

$$_{ads}(˙OH)MO|TiO_2(˙OH)_{ads} \text{ Ž } H_2O_2 \quad \text{Eq. 13}$$

In Table 3 there is a comparison of COD, TOC, CT, and CI. In the case of the COD, the lowest values in the modified $TiO_{2,nt}|Ti$ by Ir were for the Ir-Ta 50:50 (3.29 ± 1.47 mg L^{-1}); by Ru were for the Ru-Ta 50:50 (4.75 ± 0.35 mg L^{-1}) and for Ru-Ta 70:30 (5.17 ± 1.65 mg L^{-1}); and by Pb were for the Pb-Ta 30:70 (6.00 ± 1.41 mg L^{-1}) and for Pb-Ta 50:50 (6.75 ± 0.35 mg L^{-1}). In the case of TOC, CT and CI were not a major difference, they were on average 5, 5, and 0.3 mg L^{-1} respectively.

In the case of the energy consumption (Table 4), the highest values in the modified $TiO_{2,nt}|Ti$ were the Ru-Ta 30:70 and Pb-Ta 100:00 (0.223 ± 0.018 mWh m^{-3}), and the lowest were Ir-Ta 100:0 (0.018 ± 0.001 mWh m^{-3}) < $TiO_{2,nt}|Ti$ (0.031 ± 0.031 mWh m^{-3}) < Pb-Ta 70:30 (0.040 ± 0.004 mWh m^{-3}) ~ Pb-Ta 50:50 (0.041 ± 0.004 mWh m^{-3}), where the last one showed the highest removal efficiency of AMX (44.71 %, Fig. 8C) with the lowest specific energy consumption (8.69 ± 0.78 kWh Kg COD^{-1}), and the average instant current efficiency of 26.67 ± 9.19 %, in comparison with the others naked and modified surfaces of $TiO_{2,nt}|Ti$.

4. Conclusions

The results obtained in this study indicated that titania nanotubes were effectively constructed after 1h of anodization. These nanotubular structures showed a diameter of 50.10 ± 7.11 nm. From EDX analyses, the prepared TiO_2 nanotubes showed a 1:2 ratio for the Ti and O respectively, and Raman studies suggested the formation of anatase and rutile phases during anodization.

This surface was modified with a heterogeneous electrodeposited film with different concentrations of IrO_2-Ta_2O_5, RuO_2-Ta_2O_5, and PbO_2-Ta_2O_5, which increased the electroactive area and roughness compared to the ones shown by naked $TiO_{2,nt}$. SEM images showed complete coverage of all of these deposits over the nanotubes array. Ir-Ta deposits showed an electrodeposit with coliform morphology, which suggests the filling of $TiO_{2,nt}$ came out from them, as it has been reported in the literature. Ir-Ta and Pb-Ta deposits showed the biggest potential window in acidic conditions at both low and with high scan rates and Ru and Ir electrocatalysts had a similar electrochemical behavior due to their physicochemical characteristics as metallic conductivity and rutile crystalline structure.

During the electrochemical analysis, different redox processes were obtained, in the case of IrO_2-$Ta_2O_5|TiO_{2,nt}$ showed the Ir^{+2}/Ir^{+4} and Ir^{+4}/Ir^{+5}, in the case of RuO_2-$Ta_2O_5|TiO_{2,nt}$ showed the Ru^{+3}/Ru^{+4} and Ru^{+4}/Ru^{+6}, and in the case of PbO_2-$Ta_2O_5|TiO_{2,nt}$ showed the Pb^{+2}/Pb^{+3} and Pb^{+3}/Pb^{+4}. From polarization curves, 100 µA cm^{-2} was selected to be sure that electro-oxidation of AMX took place where the generation of hydroxyl radicals is developed (Herrada et al. 2018, 2020; León et al. 2020), with the highest oxidation redox state of the Ir (Eq. 6), Ru (Eq. 8) and Pb (Eq. 10). In the removal studies, the highest removal efficiency of AMX was shown with Pb-Ta 50:50 (44.71 %), which achieved the highest current densities in the polarization curve, but with a rather high COD (9 mg L^{-1}), which suggest a low degradation of AMX.

However, with the Pb-Ta 30:70, the second-highest AMX removal efficiency (38.6%) was achieved, and a low COD was obtained, which suggests a higher degradation achieved by this oxides mixture. These mixtures had a low energy consumption and specific energy consumption, with an average instant current efficiency. Although, both the Pb-Ta $50:50|TiO_{2,nt}|Ti$ and Pb-Ta $30:70 |TiO_{2,nt}|Ti$ showed effective removal efficiencies, they are lowest that reported before using IrO_2-$Ta_2O_5|Ti$ and RuO_2-$Ta_2O_5|Ti$ in acid (0.1 mol L^{-1} H_2SO_4) by the ˙OH radicals deactivation typically observed at anatase TiO_2 systems generating H_2O_2. Anyway, these kinds of materials are another alternative to be used in the electro-oxidation of AMX in acidic conditions, and it has not been reported before.

Declarations

References

1. Ahmadi A, Wu T (2020) Towards full cell potential utilization during water purification using Co/Bi/TiO_2 nanotube electrodes. Electrochim Acta 364:137272

2. Audichon T, Mayousse E, Morisset S, Morais C, Comminges C, Napporn TW, Kokoh KB (2014) Electroactivity of RuO_2-IrO_2 mixed nanocatalysts towards the oxygen evolution reaction in a water electrolyzer supplied by a solar profile. Int J Hydrogen Energy 39:16785–16796. https://doi.org/10.1016/j.ijhydene.2014.07.170

3. Auguste AFT, Quand–Meme GC, Ollo K, Mohamed B, Placide SS, Ibrahima S, Lassiné O (2016) Electrochemical oxidation of amoxicillin in its commercial formulation on thermally prepared RuO_2/Ti. J Electrochem Sci Technol 7:82–89. https://doi.org/10.5229/JECST.2016.7.1.82

4. Baheri H, Abbas A, Amin N (2016) Removal of pharmaceutical compounds from hospital wastewater using nanomaterials: a review. analytical bioanalytical chemistry research 3:1–18. https://doi.org/10.22036/abcr.2016.12655

5. Bratby J (2016) Coagulation and flocculation in water and wastewater treatment, IWA publishing. ISBN:9781780407494

6. Bavasso I, Poggi C, Petrucci E (2020) Enhanced degradation of paracetamol by combining UV with electrogenerated hydrogen peroxide and ozone. J Water Proc Engin 34:101102–110109. https://doi.org/10.1016/j.jwpe.2019.101102

7. Benjedim S, Romero-Cano LS, Pérez-Cadenas AF, Bautista-Toledo MI, Carrasco- Marín F (2020) Removal of emerging pollutants present in water using an E-coli biofilm supported onto activated carbons prepared from argan wastes. Adsorption studies in batch and fixed bed. Sci Total Environ 720:137491–137500. https://doi.org/ 10.1016/j.scitotenv.2020.137491

8. Brillas E, Sirés I, Arias C, Cabot PL, Centellas F, Rodríguez RM, Garrido JA (2005) Mineralization of paracetamol in aqueous medium by anodic oxidation with a boron – doped diamond electrode. Chemosphere 58:399–406. https://doi.org/10.1016/j.chemosphere.2004.09.028

9. Boda MA, Shah MA (2017) Fabrication mechanism of compact TiO_2 nanotubes and their photo-electrochemical ability. Mater Res Express 4:075908–075917. https://doi.org/10.1088/2053-1591/aa7cd2

10. Bueno MM, Gomez MJ, Herrera S, Hernando MD, Agüera A, Fernández-Alba AR (2012) Occurrence and persistence of organic emerging contaminants and priority pollutants in five sewage treatment plants of Spain: two years pilot survey monitoring. Environ Pollut 164:267–273. https://doi.org/10.1016/j. envpol.2012.01.038

11. Caia J, Zhoua M, Xua X, Du X (2020) Stable boron and cobalt co-doped nanotubes anode for efficient degradation of organic pollutants. J Hazard Mate 396:122723–122734. htpps://doi.org/ 10.1016/j.jhazmat.2020.122723

12. Cavalcanti EB, García–Segura S, Centellas F, Brillas E (2013) Electrochemical incineration of omeprazole in neutral aqueous medium using a platinum or boron – doped diamon anode: degradation kinetics and oxidation products. Water Res 47:1803–1815. https://doi.org/10.1016/j.watres.2013.01.002

13. Cerro-López M, Meas-Vöng Y, Méndez-Rojas MA, Martínez-Huitle CA, Quiroz MA (2014) Formation and growth of PbO_2 inside TiO_2 nanotubes for environmental applications. Appl Catal B Environ

144:174–181. https://doi.org/10.1016/j.apcatb.2013.07.018

14. Comninellis C, Vercesi GP (1991) Characterization of DSA – type oxygen evolving electrodes: choice of a coating. J Appl Electrochem 21:335–345. https://doi.org/10.1016/0040-6031(91)80257-J

15. Chen P, Cai Y, Wang J, Wang K, Tao Y, Xue J, Wang H (2018) Preparation of protonized titanate nanotubes/Fe_3O_4/TiO_2 ternary composites and dye self-sensitization for visible-light-driven photodegradation of Rhodamine B. Powder Technol 326:272–280. https://doi.org/10.1016/j.powtec.2017.12.010

16. De la Cruz N, Dantas RF, Giménez J, Esplugas S (2013) Photolysis and TiO_2 photocatalysis of the pharmaceutical propranolol: solar and artificial light. Appl Catal B Environ 130–131:249–256. https://doi.org/10.1016/j. apcatb.2012.10.003

17. Diao Y, Yan M, Li X, Zhou C, Peng B, Chen H, Zhang H (2020) *In-situ* grown of g-C_3N_4/Ti_3C_2/TiO_2 nanotube arrays on Ti meshes for efficient degradation of organic pollutants under visible light irradiation. Colloid Surf A 594:124511–124522. https://org.doi/ 10.1016/j.colsurfa.2020.124511

18. Dirany A, Sirés I, Oturan N, Ozcan A, Oturan MA (2012) Electrochemical treatment of the antibiotic sulfachloropyridazine: kinetics, reaction pathways, and toxicity evolution. Environ Sci Technol 46:4074–4082. https://doi.org/10.1021/es204621q

19. Gar AM, Tawfik A, Ookawara S (2016) Enhancement of photocatalytic activity of TiO_2 by immobilization on activated carbon for degradation of pharmaceuticals. J Environ Chem Eng 4:1929–1937. https://doi.org/10.1016/j.jece.2016.03.023

20. García–Segura S, Cavalcanti EB, Brillas E (2014) Mineralization of the antibiotic chloramphenicol by solar photoelectro-Fenton. From stirred tank reactor to solar pre-pilot plant. Appl Catal B: Environ 144:588–598. https://doi.org/10.1016/j.apcatb.2013.07.071

21. Giwa A, Yusuf A, Balogun HA, Sambudi NS, Bilad MR, Adeyemi I, Chakraborty S, Curcio S (2021) Recent advances in advanced oxidation processes for removal of contaminants from water: A comprehensive review. Proc Safety Environ Protec 146:220–256

22. González AS, Solis-Cortazar JC, Pineda-Arellano CA, Ramírez-Morales E, de los Monteros AE, Silva-Martínez S (2019) Synthesis of ruthenium-doped TiO_2 nanotube arrays for the photocatalytic degradation of terasil blue dye. J Nanosci Nanotechnol 19:5211–5219. https://doi.org/10.1166/jnn.2019.16823

23. Gopinath KP, Madhav NV, Krishnan A, Malolan R, Rangarajan G (2020) Present applications of titanium dioxide for the photocatalytic removal of pollutants from water: A review. J Environ Manage 270:110906–110932. https://doi.org/10.1016/j.jenvman.2020.110906

24. Gúlfen M, Canbaz Y, Ozdemir A (2020) Simultaneous determination of amoxicillin, Lansoprazole, and levofloxacin in pharmaceuticals by HPLC with UV - Vis detector. J Anal Test 4:45–53. https://doi.org/10.1007/s41664-020-00121-4

25. Herrada RA, Medel A, Manríquez F, Sirés I, Bustos E (2016) Preparation of IrO_2 – Ta_2O_5Ti electrodes by immersion, painting and electrophoretic deposition for the electrochemical removal of

hydrocarbons from water. J Hazard Mater 319:102–110.
https://doi.org/10.1016/j.jhazmat.2016.02.076

26. Herrada RA, Acosta-Santoyo G, Sepúlveda–Guzmán S, Brillas E, Sirés I, Bustos E (2018) IrO_2-Ta_2O_5Ti electrodes prepared by electrodeposition from different Ir:Ta ratios for the degradation of polycyclic aromatic hydrocarbons. Electrochim Acta 263:353–361. https://doi.org/10.1016/j.electacta.2018.01.056

27. Herrada RA, Rodil SE, Sepúlveda-Guzmán S, Manríquez J, Exner KS, Bustos E (2020) Characterization of Ti electrodes electrophoretically coated with IrO_2-Ta_2O_5 films with different Ir:Ta molar ratios. J Alloys Comp 862:158015–158023. https://doi.org/10.1016/j.jallcom.2020.158015

28. Hou J, Chen Z, Gao J, Xie Y, Li L, Qin S, Wang Q, Mao D, Luo Y (2019) Simultaneous removal of antibiotics and antibiotic resistance genes from pharmaceutical wastewater using the combinations of up-flow anaerobic sludge bed, anoxicoxic-oxic tank, and advanced oxidation technologies. Water Res 159:511–520. https:://doi.org/ 10.1016/j.watres.2019.05.034

29. Huang CA, Yang SW, Chen CZ, Hsu F-Y (2017) Electrochemical behavior of IrO_2-Ta_2O_5|Ti anodes prepared with different surface pretreatments of Ti substrate. Surf Coat Technol 320:270–278. https://doi.org/10.1016/j.surfcoat.2017.01.005

30. ITA (2005) International Titanium Association. Specifications Book, 4th edition, 1–44

31. Klein EY, Van Boeckel TP, Martinez EM, Pant S, Gandra S, Levin SA, Goossens H, Laxminarayan R (2018) Global increase and geographic convergence in antibiotic consumption between 2000 and 2015. Proc Natl Acad Sci 115:E3463–E3470. https://doi.org/10.1073/pnas.1717295115

32. Koiki BA, Orimolade BO, Zwane BN, Nkosi D, Mabuba N, Arotiba OA (2020) Cu_2O on anodised TiO_2 nanotube arrays: A heterojunction photoanode for visible light assisted electrochemical degradation of pharmaceuticals in water. Electrochim Acta 340:135944–135953. https://doi.org/10.1016/j.electacta.2020.135944

33. Kulkarni RM, Malladi RS, Hanagadakar MS, Doddamani MR, Santhakumari B, Kulkarni SD (2016) Ru-TiO_2 semiconducting nanoparticles for the photo-catalytic degradation of bromothymol blue. J Mater Sci Mater Electron 27:13065e13074

34. Lei X, Li X, Ruan Z, Zhang T, Pan F, Li Q, Xia D, Fu J (2018) Adsorption-photocatalytic degradation of dye pollutant in water by graphite oxide grafted titanate nanotubes. J Molecular Liquids 266:122–131

35. León I, Gomes H, Sepúlveda–Guzmán S, Cárdenas J, Rivera F, Manríquez J, Bustos E (2020) Electro-oxidation of amoxicillin using titanium electrodes electrophoretically coated by iridium or ruthenium with tantalum oxides. J Chem Technol Biotechnol. https://doi.com/10.1002/jctb.6575

36. Lin XX, Rong F, Ji X, Fu DG, Yuan CW (2011) Preparation and enhanced visible light photocatalytic activity of N-doped titanate nanotubes by loaded with Ag for the degradation of X-3B. Solid State Sci 13:1424–1428. https://doi.org/10.1016/j.solidstatesciences.2011.05.005

37. Liu G, Hoivik N, Wang K (2013) Small diameter TiO_2 nanotubes with enhanced photoresponsivity. Electrochem Commun 28:107–110

38. Mahalingam T, Velumani S, Raja M, Thanikaikarasan S, Chu JP, Wang SF, Kim YD (2007) Electrosynthesis and characterization of lead oxide thin films. Mater Charact 58:817–822. https://doi.org/10.1016/jmatchar.2006.11.021

39. Majumder A, Gupta B, Gupta AK (2019) Pharmaceutically active compounds in aqueous environment: A status, toxicity and insights of remediation. Environ Res 176:108542–108572. https://doi.org/10.1016/j.envres.2019.108542

40. Marcelino RBP, Leao MMD, Lago RM, Amorim CC (2017) Multistage ozone and biological treatment system for real wastewater containing antibiotics. J Environ Manage 195:110–116. https://doi.org/10.1016/j.jenvman.2016.04.041

41. Martínez-Sánchez C, Montiel-González F, Díaz-Cervantes E, Rodríguez-González V (2019) Unraveling the strength interaction in a TiO_2-graphene photocatalytic nanocomposite synthesized by the microwave hydrothermal method. Mater Sci Semicond Process 101:262–271

42. Michell D, Rand DA, Woods R (1978) A study of ruthenium electrodes by cyclic voltammetry and X-ray emission spectroscopy. J. Electroanal. Chem. 89, 1 (1978) 11–27, https://doi.org/10.106/S0022-0728(78)80027-8

43. Molina-Reyes J, Romero-Moran A, Uribe-Vargas H, López-Ruiz B, Sanchez-Salas JL, Ortega E, Ponce A, Morales-Sanchez A, Lopez-Huerta F, Zuñiga-Islas C (2020) Study on the photocatalytic activity of titanium. Catal Today 341:2–12. https://doi.org/10.1016/j.cattod.2018.05.033

44. Moura FC, Rios RD, Galvão BR (2018) Emerging contaminants removal by granular activated carbon obtained from residual Macauba biomass. Environ Sci Pollut Res 25:26482–26492. https://doi.org/10.1007/s11356-018-2713-8

45. Muswareen SKK, Rao MS, Sridevi G, Cole S (2019) Sol-gel synthesis of pure and TiO_2 doped $CdOFePO_4$ nanocomposites and investigation of their structural and optical properties. Mater Sci Semicond Process 102:104588

46. Naddeo V, Secondes MF, Borea L, Hasan SW, Ballesteros JF, Belgiorno V (2020) Removal of contaminants of emerging concern from real wastewater by an innovative hybrid membrane process-ultrasound, adsorption, and membrane ultrafiltration (USAMe®). Ultrason Sonochem 68:105237–1052347. https://doi.org/ 10.1016/j.ultsonch.2020.105237

47. Oh SI, Kim JC, Dar MA, Kim DW (2019) Synthesis and characterization of uniform hollow TiO_2 nanofibers using electrospun fibrous cellulosic templates for lithium- ion battery electrodes. J Alloys Compd 800:483–489

48. Olvera–Vargas H, Oturan N, Brillas E, Buisson D, Esposito B, Oturan MA (2014) Electrochemical advanced oxidation for cold incineration of the pharmaceutical ranitidine: mineralization pathway and toxicity evolution. Chemosphere 1:644–651. https://doi.org/10.1016/j.chemosphere.2014.09.084

49. Panizza M, Dirany A, Sirés I, Haidar M, Oturan N, Oturan MA (2014) Complete mineralization of the antibiotic amoxicillin by electro-Fenton with a BDD anode. J Appl Electrochem 44:1327–1335. https://doi.org/10.1007/s10800-014-0740-9

50. Peng YP, Liu CC, Chen KF, Huang CP, Chen CH (2021) Green synthesis of nano-silver-titanium nanotube array (Ag/TNA) composite for concurrent ibuprofen degradation and hydrogen generation. Chemosphere 264:128407–128418. https://doi.org/10.1016/j.chemosphere.2020.128407

51. Perrich JR (2018) Activated carbon adsorption for wastewater treatment. CRC press

52. Phoon BL, Ong CC, Saheed MSM, Show PL, Chang JS, Ling TC, Lam SS, Juan JC (2020) Conventional and emerging technologies for removal of antibiotics from wastewater. J Hazard Mater 400:122961–123061. https://doi.org/10.1016/j.jhazmat.2020.122961

53. PubChem Search. Bethesda (MD): National Center for Biotechnology Information. https://pubchem.ncbi.nlm.nih.gov/. Accessed 27 March 2021

54. Rasheed T, Adeel M, Nabeel F, Bilal M, Iqbal HMN (2019) TiO_2/SiO_2 decorated carbon nanostructured materials as a multifunctional platform for emerging pollutants removal. Sci Total Environ 688:299–311

55. Regonini D, Bowen CR, Jaroenworaluck A, Stevens R (2013) A review of growth mechanism, structure and crystallinity of anodized TiO_2 nanotubes. Mater Sci Eng Reports 74:377–406. https://doi.org/10.1016/j.mser.2013.10.001

56. Ren Z, Quan S, Gao J, Li W, Zhu Y, Liu Y, Chai B, Wang Y (2015) The electrocatalytic activity of IrO_2 – Ta_2O_5 anode materials and electrolyzed oxidizing water preparation and sterilization effect. Royal Soc Chem 5:8778–8786. https://doi.org/10.1039/C4RA14671A

57. Salazar R (2014) Degradation of a veterinary pharmaceutical product in water by electro-oxidation using a BDD anode. J Chilean Chem Soc 59:2507–2511. https://doi.org/10.4067/S0717-9707201400002000024

58. Secondes MF, Naddeo V, Belgiorno V, Ballesteros JF (2014) Removal of emerging contaminants by simultaneous application of membrane ultrafiltration, activated carbon adsorption, and ultrasound irradiation. J Hazard Mater 264:342–349. https://doi.org/10.1016/j.jhazmat.2013.11.039

59. Seo MK, Park SJ (2009) Surface characteristics of carbon fibers modified by direct oxyfluorination. J Colloid Interface Sci 330:237–242. https://doi.org/10.1016/j. jcis.2008.10.005

60. Song J, Xu Z, Liu W, Chang CT (2016) $KBrO_3$ and graphene as double hanced collaborative catalysts for the photocatalytic degradation of amoxicillin by UVA/TiO_2 nanotube processes. Mater Sci Semiconductor Proc 52:32–37

61. Sopaj F, Rodrigo MA, Oturan N, Podvorica FI, Pinson J, Oturan MA (2015) Influence of the anode material son the electrochemical oxidation efficiency. Application to oxidative degradation of the pharmaceutical amoxicillin. Chem Engin J 262:286–294. https://doi.org/10.1016/j.cej.2014.09.100

62. Sreekantan S, Lockman Z, Hazan R, Tasbihi M, Tong KL, Mohamed RA (2009) Influence of electrolyte pH on TiO_2 nanotube formation by Ti anodization. J Alloys Compd 485(1):478–483.

https://doi.org/10.1016/j.jallcom.2009.05.152

63. Subramaniam MN, Goh PS, Lau WJ, Ismail AF, Karaman M (2020) Enhanced visible light photocatalytic degradation of organicpollutants by iron doped titania nanotubes synthesized via facile one-pot hydrothermal. Power Technol 366:96–106. https://doi.org/10.1016/j.powtec.2020.02.052

64. Suhaimy SHM, Ghazali N, Arith F, Fauzi B (2020) Enhanced simazine herbicide degradation by optimized fluoride concentrations in TiO_2 nanotubes growth. Optik-Intern J Light Electron Optics 212:164651–164657. https://doi.org/10.1016/j.ijleo.2020.164651

65. Sun L, Li J, Wang CL, Li SF, Chen HB, Lin CJ (2009) An electrochemical strategy of doping Fe^{3+} into TiO_2 nanotube array films for enhancement in photocatalytic activity. Sol Energy Mater Sol Cells 93:1875–1880. https://doi.org/10.1016/j.solmat.2009.07.001

66. Tan TY, Zeng ZT, Zeng GM, Gong JL, Xiao R, Zhang P, Song B, Tang WW, Ren XY (2020) Electrochemically enhanced simultaneous degradation of sulfamethoxazole, cirpofloxacin and amoxicillin from aqueous solution by multi-walled carbon nanotube filter. Sep Pur Technol 235:116167–116174. https://doi.org/10.1016/j.seppur.2019.116167

67. Trasatti S, Petrii O (1991) Real Surface Area Measurements in Electrochemistry. Pure Appl Chem 63:711–734. https://doi.org/10.1351/pac199163050711

68. Tsai CY, Liu CW, Fan C, His HC, Chang TY (2017) Synthesis of a SnO_2/TNT heterojunction nanocomposite as a high-performance photocatalyst. J Phys Chem C 121:6050–6059. https://doi.org/10.1021/acs.jpcc.6b11005

69. Ye Y, Bruning H, Li X, Yntema D, Rijnaarts HHM (2018) Significant enhancement of micropollutant photocatalytic degradation using a TiO_2 nanotube array photoanode based photocatalytic fuel cell. Chem Engin J 354:553–562. https://doi.org/10.1016/j.cej.2018.08.064

70. Wang Y, Fenner K, Helbling DE (2020) Clustering micropollutants based on initial biotransformation for improved prediction of micropollutant removal during conventional activated sludge treatment. Environmental Science: Water Research Technology 3:554–565. https://doi.org/10.1039/c9ew00838a

71. Wang J, Wang S (2016) Removal of pharmaceuticals and personal care products (PPCPs) from wastewater: a review. J Environ Manag 182:620–640. https://doi.org/10.1016/j.jenvman.2016.07.049

72. Wang J, Zhuan R (2020) Degradation of antibiotics by advanced oxidation processes: An overview. Sci Total Environ 701:135023–135070. https://doi.org/10.1016/j.scitotenv.2019.135023

73. Wen ZH, Chen L, Meng XZ, Duan YP, Zhang ZS, Zeng EY (2014) Occurrence and human health risk of wastewater–derived pharmaceuticals in a drinking water source for Shangha, East China. Sci Total Environ 490:987–993. https://doi.org/10.1016/j.scitotenv.2014.05.087

74. Xu JC, Lu M, Guo XY, Li HL (2005) Zinc ions surface-doped titanium dioxide nanotubes and its photocatalysis activity for degradation of methyl orange in water. J Mol Catal A Chem 226:123–127.

https://doi.org/10.1016/j.molcata.2004.09.051

75. Yang C, Shang S, Li XY (2021) Fabrication of sulfur-doped TiO_2 nanotube array as a conductive interlayer of PbO_2 anode for efficient electrochemical oxidation of organic pollutants. Sep Pur Technol 258:118035–118045. https://doi.org/ 10.1016/j.seppur.2020.118035

76. Ye S, Yan M, Tan X, Liang J, Zeng G, Wu H, Song B, Zhou C, Yang Y, Wang H (2019) Facile assembled biochar-based nanocomposite with improved graphitization for efficient photocatalytic activity driven by visible light. Appl Catal B: Environ 250:78–88. https://doi.org/10.1016/j.apcatb.2019.03.004

77. Zavala Salazar NJAS (2011) Modelo cinético para el proceso de desintegración catalítica considerando la descomposición de la carga alimentaria. Instituto Politécnico Nacional, México, p 104

78. Zha SX, Cheng Y, Gao Y, Chen ZL, Megharaj M, Naidu R (2014) Nanoscale zerovalent iron as a catalyst for heterogeneous Fenton oxidation of amoxicillin. Chem Eng J 255:141–148. https://doi.org/ 10.1016/j.cej.2014.06.057

79. Zhang P, Guan BY, Yu L, Lou XW (2018) Facile synthesis of multi-shelled ZnS-CdS cages with enhanced photoelectrochemical performance for solar energy conversión. Chemistry 4:162–173. https://doi.org/10.1016/j.chempr.2017.10.018

80. Zhang H, Quan X, Chen S, Yu HT, Ma N (2009) "Mulberry-like" CdSe nanoclusters anchored on TiO_2 nanotube arrays: a novel architecture with remarkable photoelectrochemical performance. Chem Mater 21:3090–3095. https://doi.org/10.1021/cm900100k

81. Zhang J, Nosaka Y (2014) Mechanism of the OH radical generation in photocatalysis with TiO_2 of different crystalline types. J Phys Chem C 118:10824–10832. https://doi.org/10.1021/jp501214m

82. Zhang XJ, Zeng M, Zhang JW, Song AM, Lin SW (2016) Improving photoelectrochemical performance of highly-ordered TiO_2 nanotube arrays with cosensitization of PbS and CdS quantum dots. RSC Adv 6:8118–8126. https://doi.org/10.1039/C5RA22964B

83. Zhao JL, Wang XH, Chen RZ, Li TT (2005) Fabrication of titanium oxide nanotube arrays by anodic oxidation. Solid State Commun 134(10):705–710. https://doi.org/10.1016/j.ssc.2005.02.028

84. Zhou M, Li M, Hou C, Li Z, Wang Y, Xiang K, Guo X (2018) Pt nanocrystallines/TiO_2 with thickness-controlled carbon layers: preparation and activities in CO oxidation. Chin Chem Lett 29:787–790. https://doi.org/10.1016/j. cclet.2018.03.010

Tables

Table 1. SEM-EDX of naked Ti and $TiO_{2,nt}$|Ti at different times of anodization using 10 000x and 15 eV.

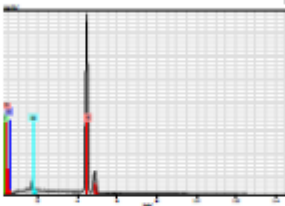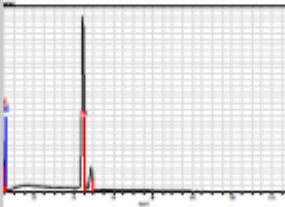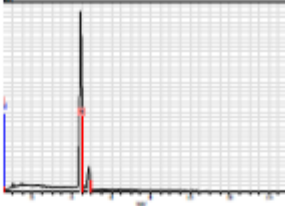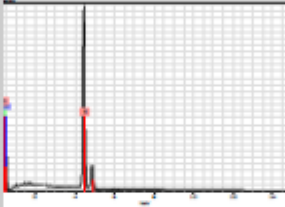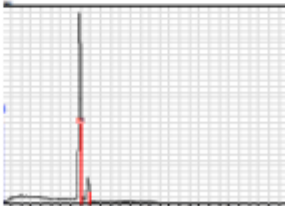| SURFACE	SPECTRA	ATOMIC PERCENTAGE			
		Ti	O	C	Si
Ti		69.21	17.03	11.24	2.52
TiO$_{2,nt}$ 1 h		29.75	68.28	1.97	-
TiO$_{2,nt}$ 2 h		27.11	66.54	6.34	-
TiO$_{2,nt}$ 3 h		27.71	67.25	5.05	-
TiO$_{2,nt}$ 4 h		27.63	67.45	4.92	-

Table 2. The capacitive current of the double layer (C_{dl}), electroactive area (A_e), and roughness (R) to different naked Ti and modified TiO$_{2,nt}$|Ti by Ir, Ru, and Pb without and with Ir, Ru, and Pb in the presence or not of Ta, considering a geometric area (A_g) of 6.9822 cm^2.

ELECTRODES	S_d (F)	A_e (cm²)	R (A_{2e}/A_g)
$IrO_2 - Ta_2O_5 \hat{e}TiO_{2,nt} \square Ti$			
Ir-Ta 100	0.00000	0.26	0.37
Ir-Ta 70:30	0.00007	0.38	0.56
Ir-Ta 50:50	0.00060	0.45	0.90
Ir-Ta 30:70	0.00040	0.23	0.58
$RuO_2 - Ta_2O_5 \hat{e}TiO_{2,nt} \square Ti$			
Ru-Ta 100:0	0.0007	0.81	1.12
Ru-Ta 70:30	0.0008	0.89	0.72
Ru-Ta 50:50	0.0008	0.34	0.93
Ru-Ta 30:70	0.0007	0.54	0.65
$PbO_2 - Ta_2O_5 \hat{e}TiO_{2,nt} \square Ti$			
Pb-Ta 100:0	0.0002	0.89	0.86
Pb-Ta 70:30	0.0030	0.27	0.54
Pb-Ta 50:50	0.0030	0.21	0.53
Pb-Ta 30:70	0.0060	0.48	0.94
$Ta_2O_5 \hat{e}TiO_{2,nt} \square Ti$			
Ta	0.0007	0.15	0.60
$TiO_{2,nt}$	0.0030	0.20	0.45
Ti	0.0050	0.30	0.72

Table 3. Chemical organic demand (COD), total organic carbon (TOC), carbon total (CT) and carbon inorganic (CI) of AMX in 0.1 mol L^{-1} H_2SO_4 after 120 min in presence of different naked Ti and modified $TiO_{2,nt}$|Ti by Ir, Ru and Pb without and with Ir, Ru and Pb in presence or not of Ta.

ELECTRODES	COD (mg L^{-1})	TOC (mg L^{-1})	CT (mg L^{-1})	Cl (mg L^{-1})
AMX	11.50 ± 0.71	4.91 ± 0.01	5.18 ± 0.01	0.27 ± 0.01
IrO$_2$ – Ta$_2$O$_5$ êTiO$_{2,nt}$ ⫫Ti				
Ir-Ta 100:0	9.50 ± 0.71	5.55 ± 0.26	5.83 ± 0.22	0.28 ± 0.04
Ir-Ta 70:30	9.67 ± 1.41	4.74 ± 0.42	5.06 ± 0.41	0.32 ± 0.01
Ir-Ta 50:50	3.29 ± 1.47	5.65 ± 0.35	5.96 ± 0.36	0.31 ± 0.01
Ir-Ta 30:70	10.00 ± 0.1	5.56 ± 0.45	5.84 ± 0.45	0.27 ± 0.01
RuO$_2$ – Ta$_2$O$_5$ êTiO$_{2,nt}$ ⫫Ti				
Ru-Ta 100:0	11.50 ± 2.83	4.45 ± 0.20	4.79 ± 0.19	0.34 ± 0.01
Ru-Ta 70:30	5.17 ± 1.65	4.25 ± 0.40	4.61 ± 0.38	0.36 ± 0.02
Ru-Ta 50:50	4.75 ± 0.35	4.20 ± 0.03	4.56 ± 0.04	0.36 ± 0.01
Ru-Ta 30:70	11.25 ± 0.35	5.29 ± 0.96	5.58 ± 1.02	0.29 ± 0.06
PbO$_2$ – Ta$_2$O$_5$ êTiO$_{2,nt}$ ⫫Ti				
Pb-Ta 100:0	8.75 ± 0.35	4.95 ± 0.33	5.27 ± 0.28	0.32 ± 0.05
Pb-Ta 70:30	10.00 ± 0.01	5.63 ± 0.44	5.94 ± 0.46	0.31 ± 0.02
Pb-Ta 50:50	6.75 ± 0.35	5.43 ± 0.07	5.77 ± 0.02	0.34 ± 0.05
Pb-Ta 30:70	6.00 ± 1.41	4.88 ± 0.38	5.16 ± 0.42	0.28 ± 0.05
Ta$_2$O$_5$ êTiO$_{2,nt}$ ⫫Ti				
Ta	7.00 ± 1.41	4.20 ± 0.22	4.54 ± 0.20	0.34 ± 0.03
TiO$_{2,nt}$	10.00 ± 0.01	5.11 ± 0.01	5.37 ± 0.01	0.26 ± 0.01
Ti	2.00 ± 0.01	4.21 ± 0.01	4.57 ± 0.01	0.36 ± 0.01

Table 4. Energy consumption (EC), specific energy consumption (E$_{sp}$), and instant current efficiency (ICE) of AMX in 0.1 mol L^{-1} H$_2$SO$_4$ after 120 min in presence of different naked Ti and modified TiO$_{2,nt}$|Ti by Ir, Ru, and Pb without and with Ir, Ru, and Pb in the presence or not of Ta.

| ELECTRODES	EC (Wh m^{-3})	E$_{sp}$ (kWh Kg COD^{-1})	ICE (%)
IrO$_2$ – Ta$_2$O$_5$ ê TiO$_{2,nt}$ ▯Ti			
Ir-Ta 100:0	0.018 ± 0.001	9.04 ± 0.11	14.13 ± 3.99
Ir-Ta 70:30	0.152 ± 0.060	83.46 ± 6.48	56.51 ± 3.13
Ir-Ta 50:50	0.069 ± 0.026	9.38 ± 1.88	46.64 ± 1.36
Ir-Ta 30:70	0.056 ± 0.022	41.32 ± 7.78	47.84 ± 4.39
RuO$_2$ – Ta$_2$O$_5$ ê TiO$_{2,nt}$ ▯Ti			
Ru-Ta 100:0	0.134 ± 0.087	63.46 ± 6.90	51.70 ± 2.18
Ru-Ta 70:30	0.130 ± 0.001	20.48 ± 0.22	28.18± 2.84
Ru-Ta 50:50	0.194 ± 0.062	28.76 ± 2.12	17.07± 3.80
Ru-Ta 30:70	0.223 ± 0.018	96.37 ± 0.70	43.15 ± 1.13
PbO$_2$ – Ta$_2$O$_5$ ê TiO$_{2,nt}$ ▯Ti			
Pb-Ta 100:0	0.223 ± 0.018	81.19 ± 6.53	29.44 ± 5.69
Pb-Ta 70:30	0.040 ± 0.004	26.90 ± 2.53	10.87 ± 6.33
Pb-Ta 50:50	0.041 ± 0.004	8.69 ± 0.78	26.67± 9.19
Pb-Ta 30:70	0.090 ± 0.008	16.42 ± 1.41	56.98 ± 0.07
Ta$_2$O$_5$ ê TiO$_{2,nt}$ ▯Ti			
Ta	0.146 ± 0.042	35.08 ± 5.08	19.47 ± 6.11
TiO$_{2,nt}$	0.031 ± 0.010	20.85 ± 0.01	23.19 ± 3.51
Ti	0.024 ± 0.010	25.66 ± 0.10	20.64 ± 4.31

Figures
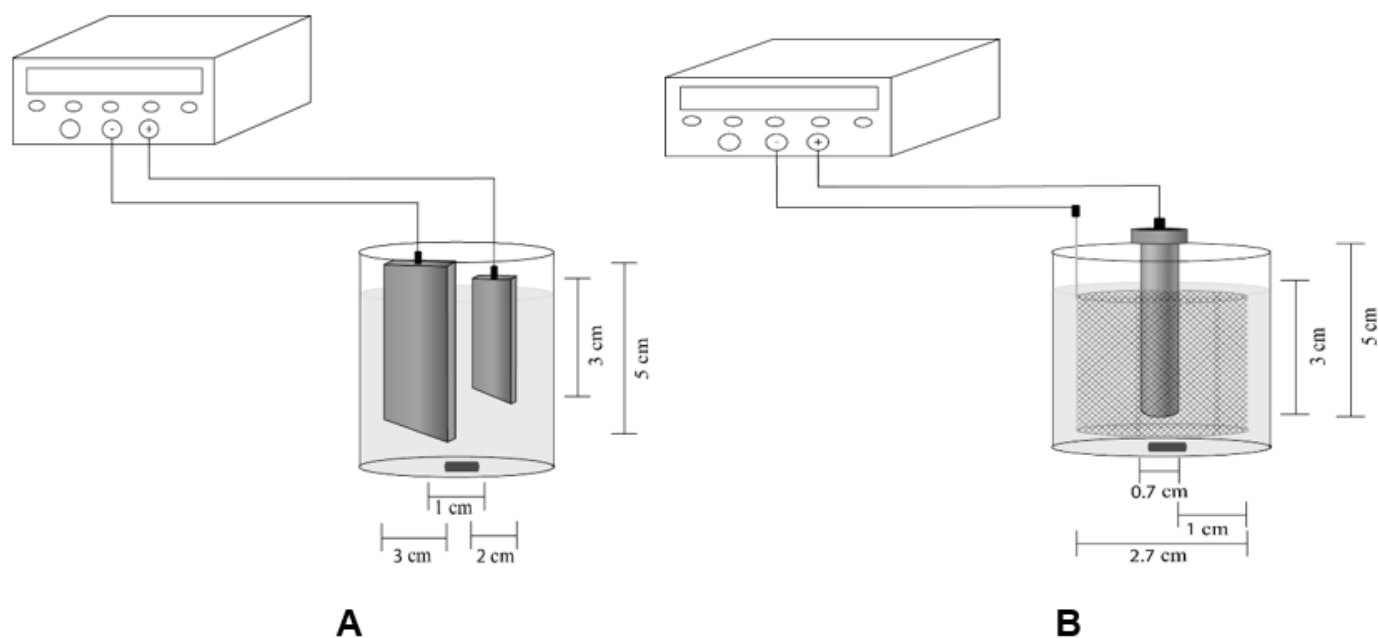
Figure 1

Two electrodes electrochemical cell using Ti plate (A) or cylinder (B) for the electrophoretic anodization to obtain TiO2,nt.
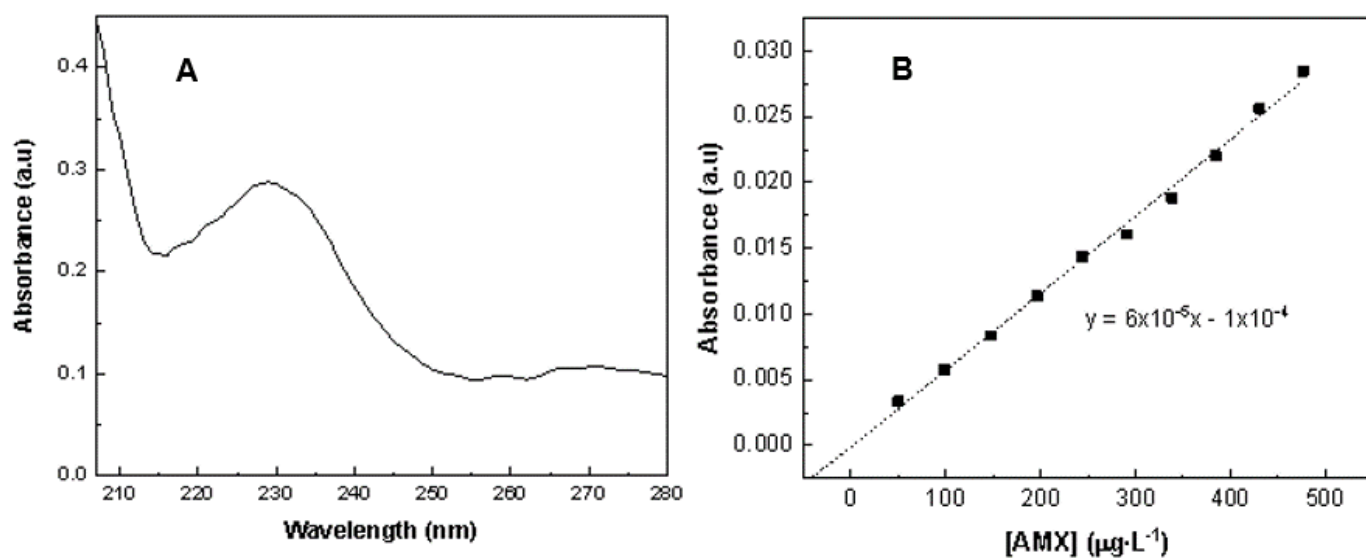

Figure 2

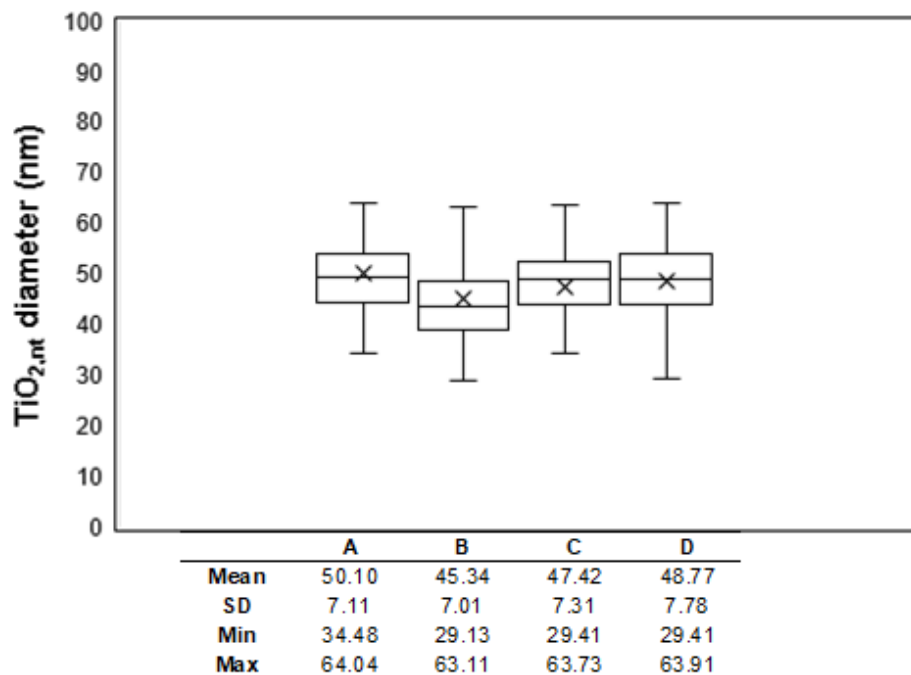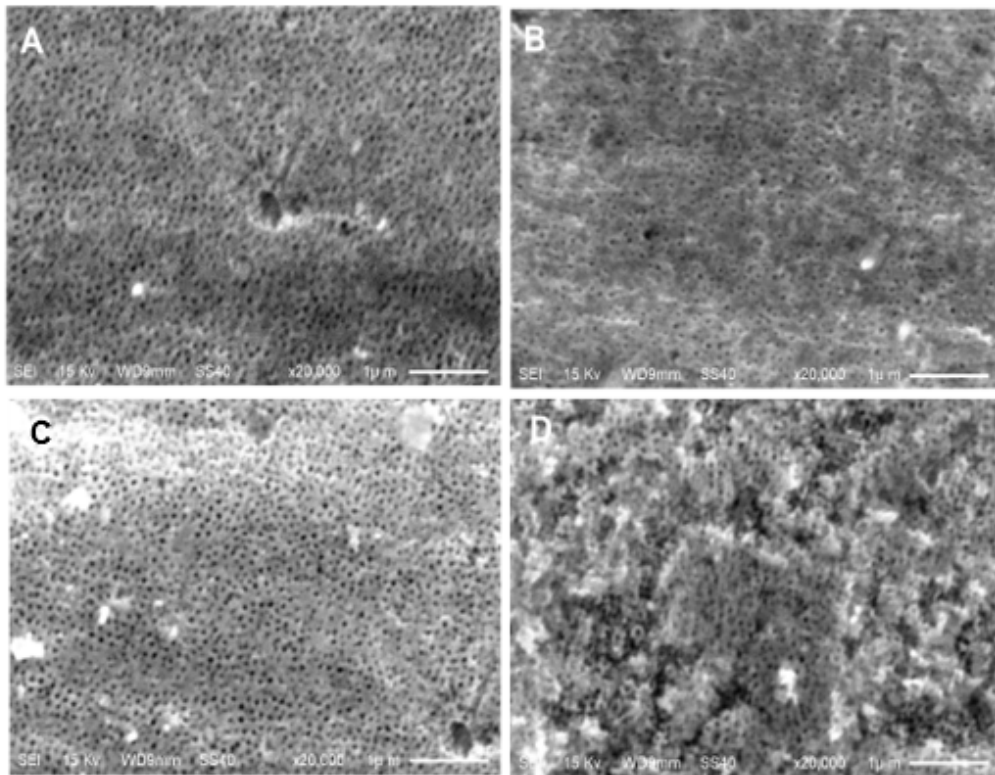UV-Vis signals of AMX (A) used to the calibration curve (B) in 0.1 mol L-1 H2SO4 by spectroscopy.

	A	B	C	D
Mean	50.10	45.34	47.42	48.77
SD	7.11	7.01	7.31	7.78
Min	34.48	29.13	29.41	29.41
Max	64.04	63.11	63.73	63.91

Figure 3

SEM of modified TiO2,nt at different anodization times using 10 000 x and 15 eV: 1 h (A), 2 h (B), 3 h (C) and 4 h (D) with the corresponding statistical of the TiO2,nt diameter of 100 nanotubes measured by the software ImageJ 1.46r from Wayne Rasband, National Institutes of Health, USA.
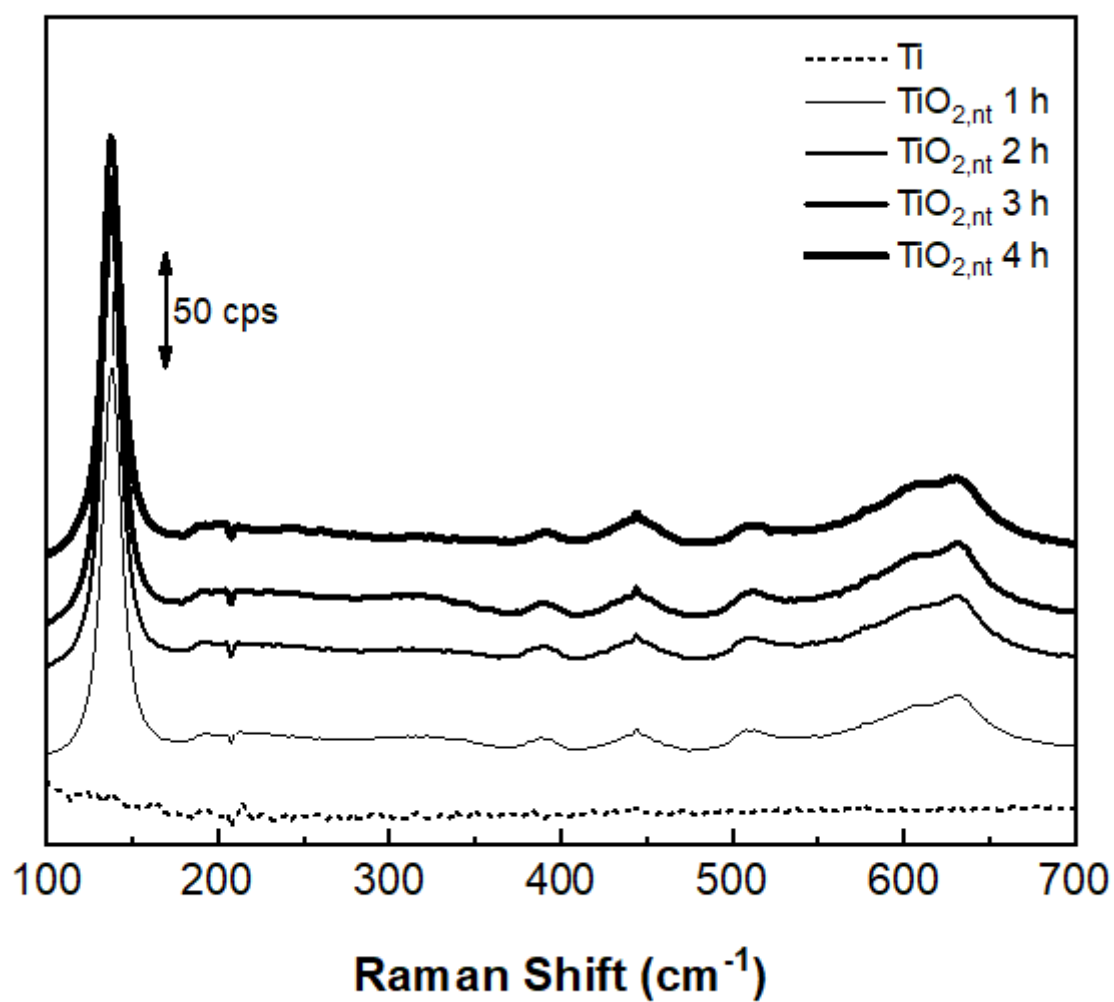
Figure 4

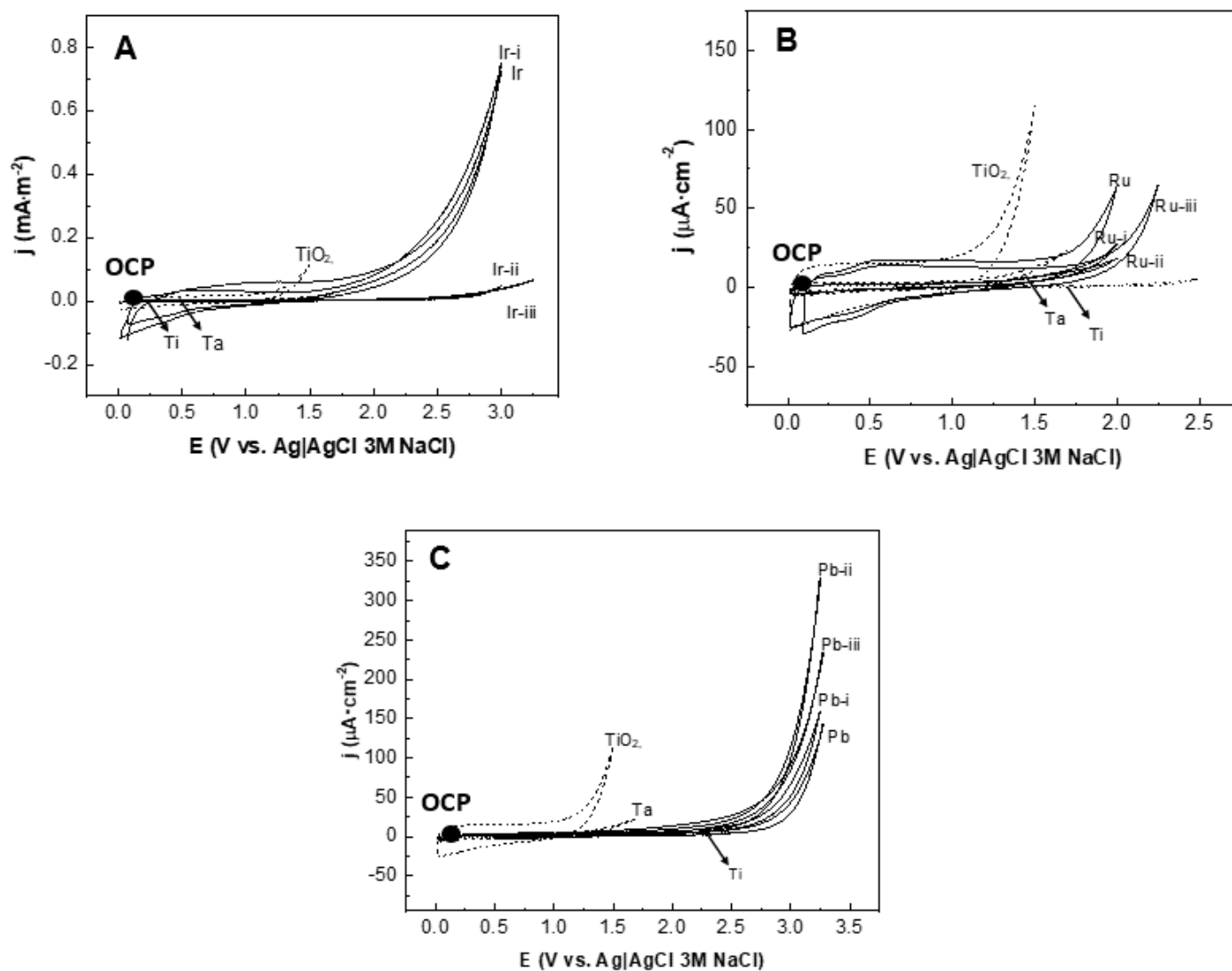Raman spectra of modified TiO2,nt at different anodization times.

Figure 5

Cyclic voltammetry of naked Ti and modified TiO2,nt|Ti by the different concentration relations of Ir (A), Ru (B) and Pb (C) without and with Ta with the concentration relation of 30:70 (i), 50:50 (ii), 70:30 (iii) electrodes in 0.1 mol L-1 H2SO4 at 20 mV s-1 and 293 K.
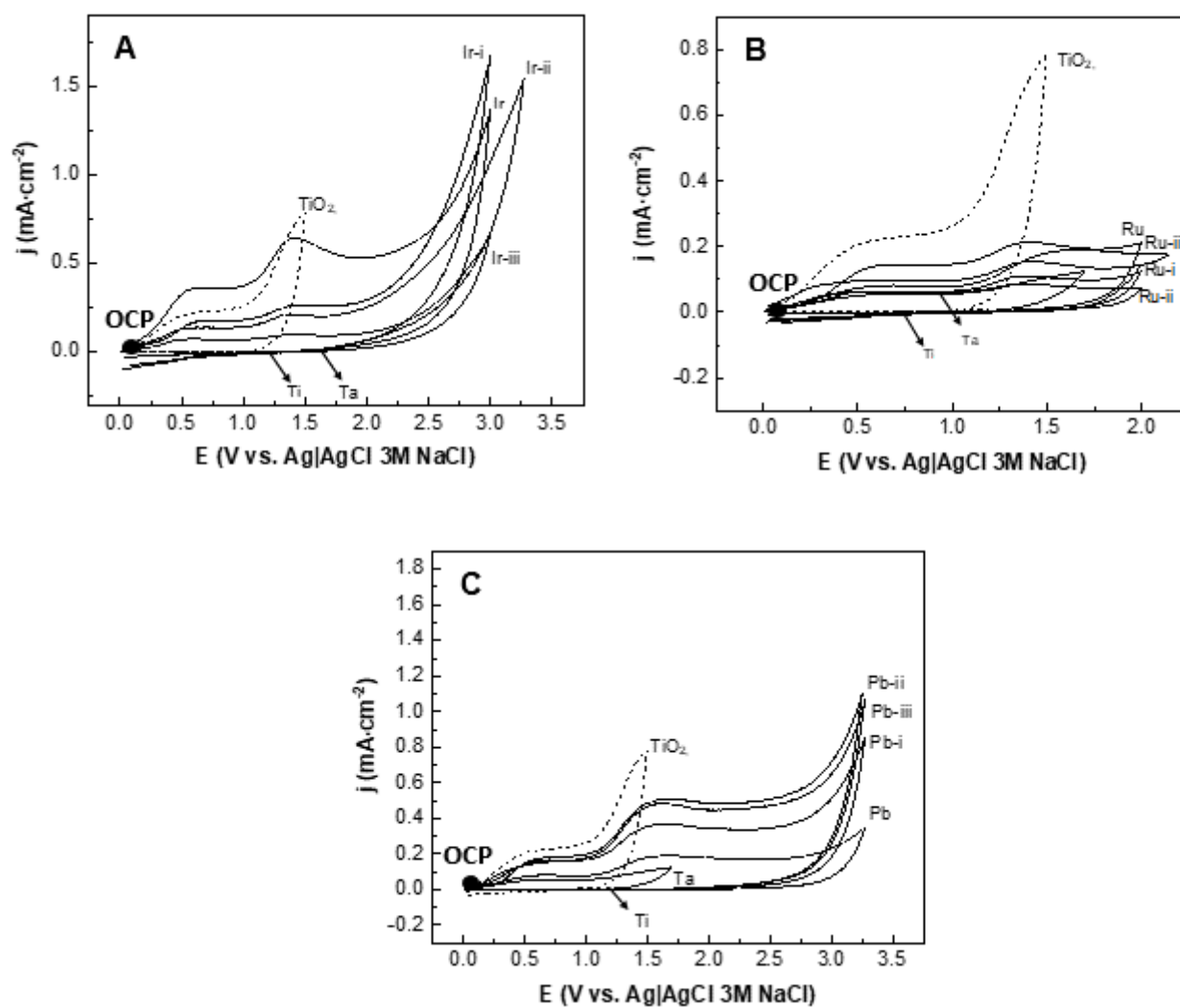
Figure 6

Cyclic voltammetry of naked Ti and modified TiO2,nt|Ti by the different concentration ratios of Ir (A), Ru (B) and Pb (C) without and with Ta with the concentration ratio of 30:70 (i), 50:50 (ii), 70:30 (iii) electrodes in 0.1 mol L-1 H2SO4 at 200 mV s-1 and 293 K.
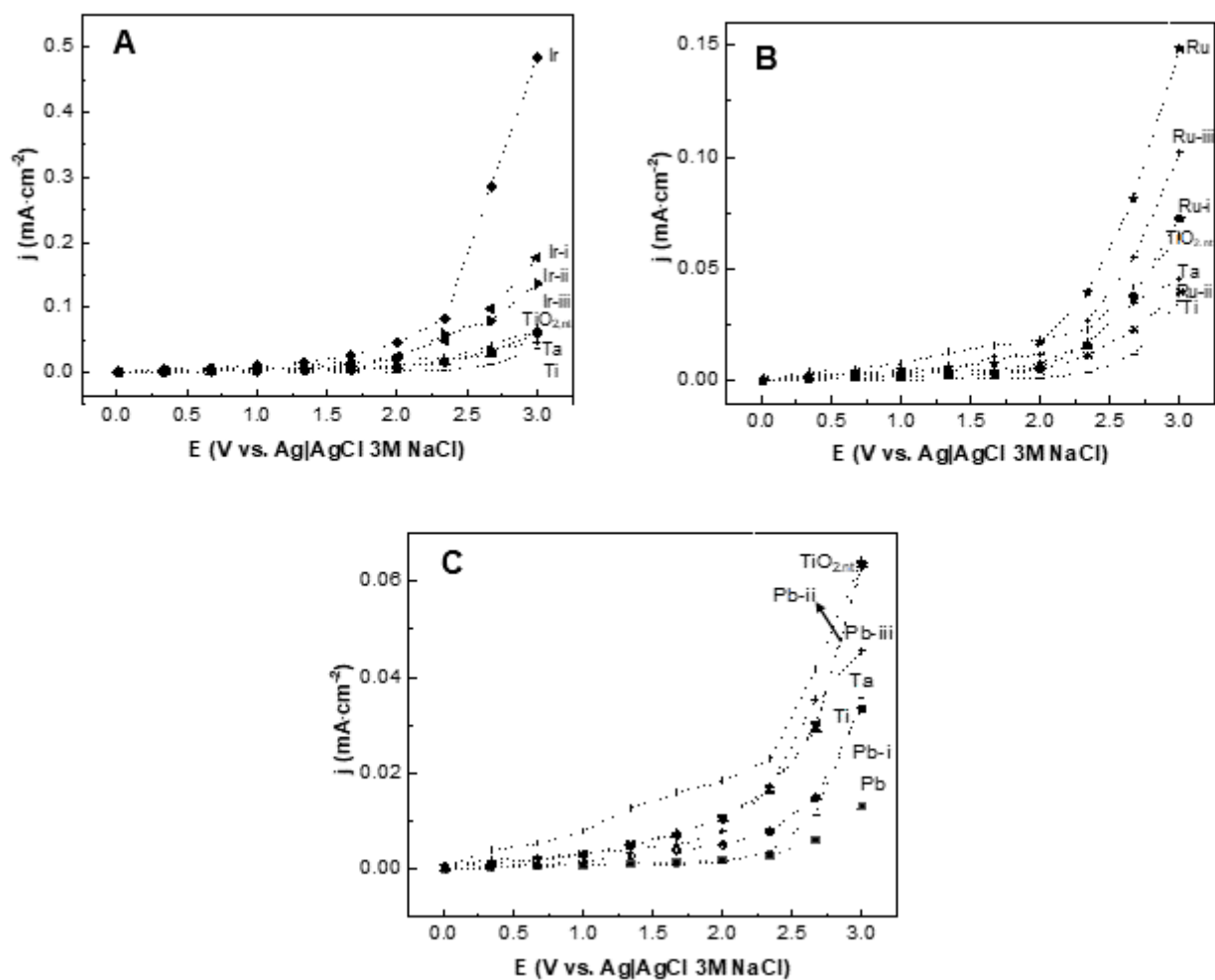
Figure 7

Polarization curves of AMX in 0.1 mol L-1 H2SO4 using cronoamperometries by 15 min in presence of naked Ti and modified TiO2,nt|Ti by the different concentration ratios of Ir (A), Ru (B), and Pb (C) without and with Ta with the concentration ratio of 30:70 (i), 50:50 (ii), 70:30 (iii) electrodes at 293 K.
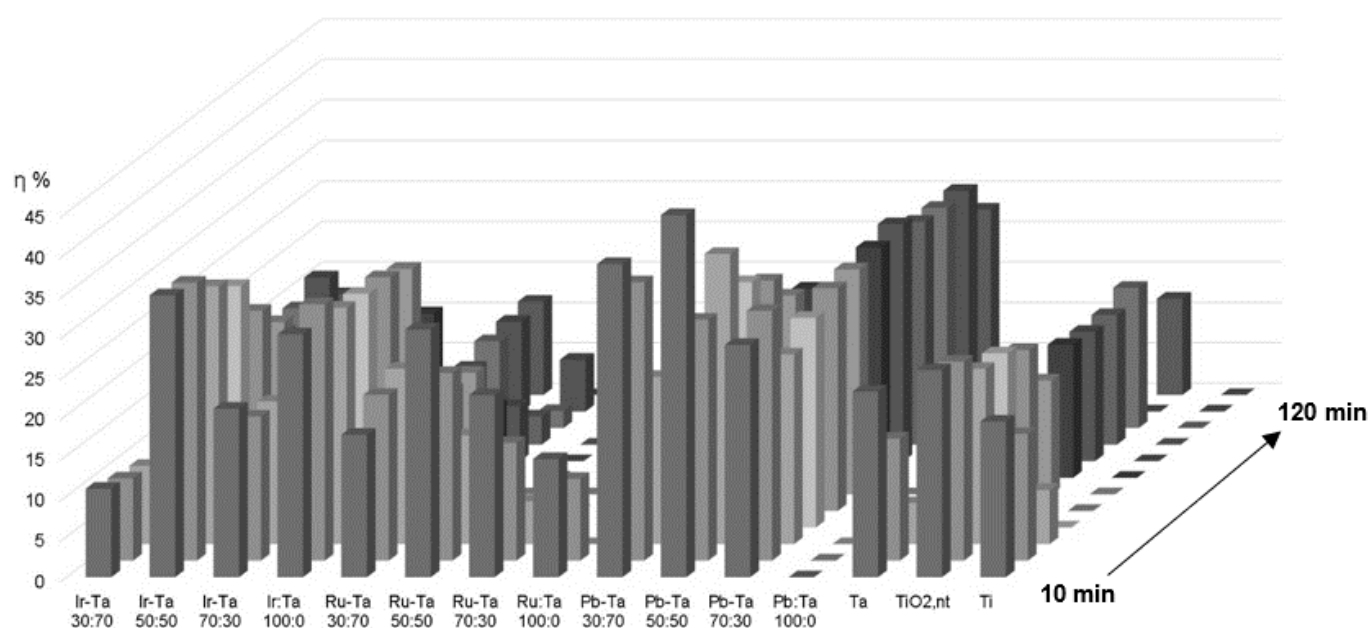
Figure 8

Degradation efficiencies of AMX in 0.1 mol L-1 H2SO4 every 10 min to 120 min of electrolysis using naked Ti and modified TiO2,nt|Ti by the different concentration relations of Ir (A), Ru (B), and Pb (C) without and with Ta with the concentration relation of 30:70, 50:50 and 70:30 electrodes at 293 K.